

Path planning of magnetic microswimmers in high-fidelity simulations of capillaries with deep reinforcement learning

Lucas Amoudruz¹, Sergey Litvinov¹, and Petros Koumoutsakos^{1,*}

¹School of Engineering and Applied Sciences, Harvard University, Cambridge, MA 02138, United States.

*corresponding author: petros@seas.harvard.edu

April 4, 2024

Abstract

Biomedical applications such as targeted drug delivery, microsurgery or sensing rely on reaching precise areas within the body in a minimally invasive way. Artificial bacterial flagella (ABFs) have emerged as potential tools for this task by navigating through the circulatory system. While the control and swimming characteristics of ABFs is understood in simple scenarios, their behavior within the bloodstream remains unclear. We conduct simulations of ABFs evolving in the complex capillary networks found in the human retina. The ABF is robustly guided to a prescribed target by a reinforcement learning agent previously trained on a reduced order model.

1 Introduction

Targeted drug delivery, micro-surgery and micro-sensing represent important areas of research aimed at revolutionizing precision medicine. These challenging tasks require precise access to target areas in the body, which are often difficult to reach in a non-invasive way. Over the past decade, artificial microswimmers have emerged as potent candidates for navigating to specific regions of the human body through the circulatory system or tissues [1]. A particular form of artificial microswimmers, known as artificial bacterial flagella (ABFs), features a corked-screw shaped body propelled by rotating magnetic fields [2]. ABFs have been utilized in various applications, including the navigation through bovine eye tissues ex-vivo [3], assisting spermatozoa in reaching oocytes [4], enhancing nanoparticle transport [5] and carrying drugs for cancer therapy [6].

The swimming properties of ABFs are well understood in the idealized scenario of unbounded viscous fluids [7, 8]. Venugopalan et al. demonstrated that ABFs can propel in low concentrated blood suspensions [9]. Alapan et al. have guided micro-rollers in physiologically relevant blood concentrations with a rotating magnetic field [10]. Qi et al. have conducted numerical simulations of these rollers through blood in straight pipes [11]. However, the swimming characteristics of ABFs within the bloodstream have not been thoroughly investigated. The control of microswimmers for path planning have been the subject of recent advances with the emergence of reinforcement learning (RL). Muiños-Landin et al. used RL in an experimental setup to control a microswimmer towards a target, with no background flow [12]. Similarly, several studies applied RL to guide a single [13, 14, 15, 16, 17] or multiple [18] swimmers towards a target in the presence of a background flow with the help of numerical simulations. Yang et al. achieved path-planning of point particles between obstacles represented by red blood cells (RBCs) [19]. However the numerical models used in these studies do not reflect the complex flow patterns present in capillaries, the finite size of the swimmer, and the presence of deformable blood cells.

In this work, we model and simulate an ABF evolving in a capillary network typically found in the retina. In particular, we aim to learn a control strategy that guides the ABF to a prescribed target by varying the external magnetic field. The geometric representation of the environment is reproduced from a fundus image of a retinal capillary network [20]. The simulations include an accurate RBC model that was extensively validated on experimental data [21], coupled with the dissipative particle dynamics (DPD) method to resolve the hydrodynamics at the microscale [22]. The control policy to guide the ABF to its target is learned with RL. To substantially reduce the computational cost, the RL agent is trained on a reduced order model of the high-fidelity simulations.

2 Methods

The simulations consist of an ABF evolving through a network of capillaries filled with blood at a hematocrit $Ht = 25\%$. The ABF has a radius of $2\ \mu\text{m}$ and a length of $18.37\ \mu\text{m}$, within the range of the ABFs presented in the literature. Blood is modeled as RBC membranes suspended in the plasma and enclosing the cytosol, a fluid 5 times more viscous than the plasma. Both the plasma and the cytosol are viscous Newtonian fluids and are modeled with the DPD method [22]. RBC membranes evolve according to bending forces, and shear forces that are zero when the membrane takes the shape of the stress-free state of the RBC cytoskeleton. In addition, area and volume of the RBC membranes are constrained through penalization forces. The details of the model and its parameters are described in Amoudruz et al. , where the model has been extensively validated against experimental data [21]. The ABF is represented as a set of frozen particles and a surface moving as a rigid body. The surrounding solvent particles interact with the ABF particles through DPD forces and are bounced-back from the surface. The magnetic moment \mathbf{m} of the ABF remains constant in the frame of reference of the swimmer, perpendicular to its principal axis. The ABF is immersed in an external, uniform magnetic field \mathbf{B} , and experiences a magnetic torque $\mathbf{T} = \mathbf{m} \times \mathbf{B}$. This torque, combined with the cork-screw shape of the ABF’s tail, causes the ABF to propel along its main axis [7]. The external magnetic field varies over time and will be the controlled quantity used to stir the ABF towards its target.

The boundaries of the capillaries were generated from a human retinal vasculature fundus image in Ghassemi et al. [20] (see supplementary material). The walls are formed by a layer of frozen DPD particles, of width larger than the interaction cutoff. Furthermore, the DPD particles are bounced-back from the wall surface. The parameters of the DPD forces and interactions between every objects of the simulations are detailed in Amoudruz [23]. To drive the flow, an external body force is applied to the DPD particles, following the approach described in Yazdani et al. [24]. The body force is derived from the pressure gradient of the flow previously solved by an external CFD package. We use *Aphros* [25] to solve the Stokes equation in the retina geometry, assuming a Newtonian fluid and a constant velocity at the inlet. In the blood simulations, the body forces were scaled to match a given Reynolds number at the inlet of the domain. The blood simulations are performed with *Mirheo* [26], a high-performance package for microfluidics simulations on multi-GPU architectures.

3 Results

3.1 Control via reinforcement learning

We consider the task of bringing the ABF from the entry of the retinal capillary network to a given target by varying the external magnetic field. RL algorithms typically require thousands to millions of episodes and it is thus intractable to directly interact with the high-fidelity model, which requires 64 P100 GPUs over 24 hours per simulation. Instead, we use a reduced order model to train a policy that we then apply to the high-fidelity model. The reduced order model consists of a self-propelling point particle advected by a background velocity field \mathbf{u} . The point particle represents the center of mass of the ABF and the background velocity is obtained from the grid-based solver *Aphros*. In addition, we model the collisions with surrounding

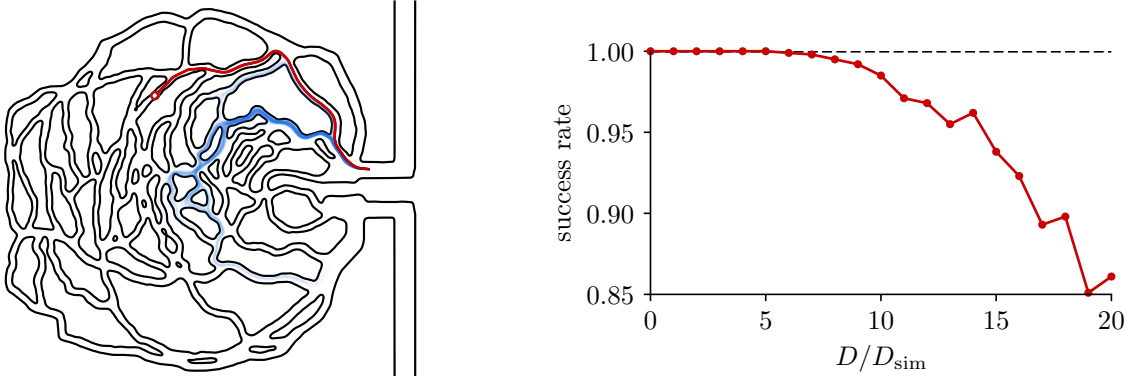


Figure 1: Left: Trajectories of passive tracers (blue) and controlled swimmers (red) obtained from 100 random seeds, with the reduced order model and $D = D_{\text{sim}}$. The circle represents the target. Right: Success rate of the control policy against the noise level D relative to that measured from the high-fidelity simulations D_{sim} .

RBCs via a stochastic term, resulting in the stochastic differential equation (SDE)

$$\dot{\mathbf{x}} = \mathbf{u}(\mathbf{x}) + U\mathbf{p} + \sqrt{D}\boldsymbol{\xi}, \quad (1)$$

where \mathbf{p} and U are the self-propelling velocity direction and magnitude of the ABF, respectively. D is a diffusion coefficient, and $\boldsymbol{\xi}$ is a vector of Gaussian white noise. In addition, the particle is bounced-back from the wall boundaries. The parameters D and U were calibrated from the high-fidelity blood simulation (see supplementary material).

The system is advanced in time with a piece-wise constant action \mathbf{p} , updated every Δt units of time. The direction \mathbf{p} is computed from the ABF’s position \mathbf{x} through the control policy. Each episode is ended if either the simulation time exceeds a maximal time T_{max} or if the ABF reaches the target within a distance δ . The reward at step t is expressed as

$$r_t = -C\Delta t + \|\mathbf{x}_{t-1} - \mathbf{x}_{\text{target}}\| - \|\mathbf{x}_t - \mathbf{x}_{\text{target}}\|, \quad (2)$$

where $C > 0$ is a constant and $\mathbf{x}_{\text{target}}$ is the target position. The first term in eq. (2) penalizes long trajectories, while the second term is a reward shaping that is positive when the ABF progresses towards its target [27].

We train the policy using V-racer [28], an actor-critic off-policy RL algorithm that was applied to falling objects [29], magnetic microswimmers [18] and self-propelling fish [30, 31]. The algorithm is implemented in *Korali* [32]. Each episode consists of about 500 experiences, and we train the agent over 10 000 episodes.

The trajectories obtained with the reduced order model are shown on fig. 1 and compared to those obtained with passive tracers. We note that passive tracers are much more sensitive to the noise than the controlled swimmers. Furthermore, the passive tracers do not reach the target, as opposed to the swimmers controlled with RL.

To assess the robustness of the control policy, we vary the noise level D and measure the number of times the particle reached its target out of 1000 trajectories. We define the success rate as the ratio of these two quantities. Figure 1 demonstrates that the control policy brings the swimmer to its target more than 98% of the time when $D < 10D_{\text{sim}}$. Increasing the noise level further results in a lower success rate. However, the success rate remains above 85% when $D \leq 20D_{\text{sim}}$. In comparison, passive particles never reach the target for any values $D \in [0, 20D_{\text{sim}}]$.

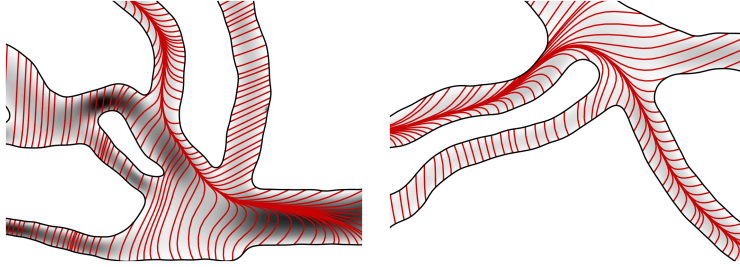


Figure 2: Streamlines of the policy at bifurcations. The direction chosen by the agent is parallel to these streamlines.

Figure 2 shows the policy at a bifurcation. The streamlines of the directions obtained from the policy converge to a line that connects the starting point to the target. This line seems to favor regions where the background velocity is larger and aligned with the swimming direction, thus decreasing the overall travel time of the swimmer. When the swimmer is away from this line, the agent chooses a direction that brings the swimmer back to the line. This mechanism explains the robustness of the control policy to external perturbations.

3.2 Control in high-fidelity blood simulations

We now apply the control policy trained on the reduced order model to the high-fidelity model. The policy maps the swimmer’s position to a swimming direction \mathbf{p} . Since the swimming direction of ABFs is perpendicular to the plane of rotation of the magnetic field, we set

$$\mathbf{B}(t) = BR_x(\mathbf{p}) \begin{pmatrix} 0 \\ \cos \omega t \\ \sin \omega t \end{pmatrix}, \quad (3)$$

where B and ω are the magnitude and frequency of rotation of the magnetic field, respectively, and $R_x(\mathbf{p})$ is the rotation that transforms the vector \mathbf{e}_x into the swimming direction \mathbf{p} with axis of rotation $\mathbf{e}_x \times \mathbf{p}$. The direction \mathbf{p} is computed from the policy evaluated at the ABF’s center of mass, and the magnetic field is adapted at every time step of the simulation.

Figure 3 shows that the ABF reaches its target with the policy learned from the reduced order model. The ABF follows a trajectory very similar to that obtained with the reduced order model. Furthermore, the ABF tends to align with the flow direction and the capillaries’ centerline, indicating that the ABF swims along the flow to reduce its travel time. Away from bifurcations, the policy seems to keep the ABF near the center of the capillaries, where the flow is faster. We observe that the ABF stays closer to the wall boundaries in the vicinity of bifurcations. This strategy can have two benefits: the ABF is closer to the correct downstream branch, and the ABF has a larger swimming speed relative to the flow, allowing a finer control in these critical areas.

We emphasize that the policy was trained on an environment that is different than the high-fidelity simulations but has a similar qualitative response. In the reduced order model, we assume that the swimmer reorients instantaneously to the control output, which is not the case in the high-fidelity blood model. Furthermore, the velocity field is different than that obtained from the stokes solver with the Newtonian assumption. Finally, the swimming speed of the ABF with respect to the fluid depends on the local hematocrit, the configuration of the surrounding RBCs and the geometry of the capillaries, which we ignore in the reduced order model. Despite these approximations, the policy learned by RL is successful in the high-fidelity simulations, indicating that RL is an effective method to learn policies that are robust to variations in the environment.

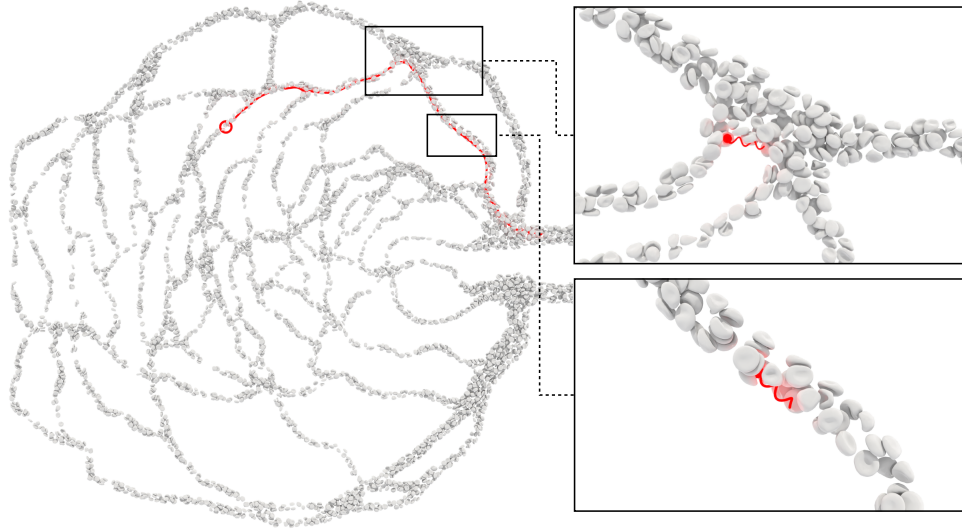


Figure 3: Trajectory of the ABF in the blood simulations with feedback control via the RL policy. The ABF reaches the target (red circle) and follows a trajectory (red line) similar to that obtained with the reduced order model. The zoomed-in views show the ABF swimming in the capillaries.

4 Summary

We have conducted, for the first time, high-fidelity simulations of ABFs evolving in the bloodstream through complex capillaries. The simulations employ a high-fidelity blood model coupled with the DPD method to resolve the flow mechanics. The ABF is propelled via an external magnetic field, which is controlled by a RL agent with the aim of guiding the ABF towards a prescribed target. The agent was trained on a reduced order model that was calibrated from the blood simulations. This approach is far less computationally expensive than using the blood simulations during training and only requires the geometric representation of the capillaries. The control policy is robust to external noise in the reduced order environment. Strikingly, it successfully guides the swimmer to its target in the high-fidelity blood simulations.

The presented approach is a candidate of choice for designing control methods in real conditions, and requires only a moderate computational cost as the RL agent is trained on reduced order models rather than the costly, high-fidelity ones. Finally, this approach can be used for personalized control policy as the geometric representation of the capillary networks was generated from fundus images. This method can serve for the navigation of microswimmers in the context of targeted drug delivery or microsurgery at precise locations, and may constitute a crucial tool for precision medicine.

Acknowledgments

We acknowledge the computational resources granted by the Swiss National Supercomputing Center (CSCS) under the project ID “s1160”.

Conflicts of Interest

The authors have no conflicts to disclose.

References

- [1] Ada-Ioana Bunea and Rafael Taboryski. Recent advances in microswimmers for biomedical applications. *Micromachines*, 11(12):1048, 2020.
- [2] Rémi Dreyfus, Jean Baudry, Marcus L Roper, Marc Fermigier, Howard A Stone, and Jérôme Bibette. Microscopic artificial swimmers. *Nature*, 437(7060):862–865, 2005.
- [3] Jiangfan Yu, Dongdong Jin, Kai-Fung Chan, Qianqian Wang, Ke Yuan, and Li Zhang. Active generation and magnetic actuation of microrobotic swarms in bio-fluids. *Nature communications*, 10(1):5631, 2019.
- [4] Mariana Medina-Sánchez, Lukas Schwarz, Anne K Meyer, Franziska Hebenstreit, and Oliver G Schmidt. Cellular cargo delivery: Toward assisted fertilization by sperm-carrying micromotors. *Nano letters*, 16(1):555–561, 2016.
- [5] Simone Schuerle, Ava P Soleimany, Tiffany Yeh, GM Anand, M Häberli, HE Fleming, Nima Mirkhani, Famin Qiu, Sabine Hauert, X Wang, et al. Synthetic and living micropropellers for convection-enhanced nanoparticle transport. *Science advances*, 5(4):eaav4803, 2019.
- [6] Xu Wang, Jun Cai, Lili Sun, Shuo Zhang, De Gong, Xinghao Li, Shuhua Yue, Lin Feng, and Deyuan Zhang. Facile fabrication of magnetic microrobots based on spirulina templates for targeted delivery and synergistic chemo-photothermal therapy. *ACS applied materials & interfaces*, 11(5):4745–4756, 2019.
- [7] Li Zhang, Jake J Abbott, Lixin Dong, Bradley E Kratochvil, Dominik Bell, and Bradley J Nelson. Artificial bacterial flagella: Fabrication and magnetic control. *Applied Physics Letters*, 94(6), 2009.
- [8] Li Zhang, Jake J Abbott, Lixin Dong, Kathrin E Peyer, Bradley E Kratochvil, Haixin Zhang, Christos Bergeles, and Bradley J Nelson. Characterizing the swimming properties of artificial bacterial flagella. *Nano letters*, 9(10):3663–3667, 2009.
- [9] Pooyath Lekshmy Venugopalan, Ranajit Sai, Yashoda Chandorkar, Bikramjit Basu, Srinivasrao Shivashankar, and Ambarish Ghosh. Conformal cytocompatible ferrite coatings facilitate the realization of a nanovoyager in human blood. *Nano letters*, 14(4):1968–1975, 2014.
- [10] Yunus Alapan, Ugur Bozuyuk, Pelin Erkoç, Alp Can Karacakol, and Metin Sitti. Multifunctional surface microrollers for targeted cargo delivery in physiological blood flow. *Science robotics*, 5(42):eaba5726, 2020.
- [11] Xiaojing Qi, Shuo Wang, Shuhao Ma, Keqin Han, Xin Bian, and Xuejin Li. Quantitative prediction of rolling dynamics of leukocyte-inspired microroller in blood flow. *Physics of Fluids*, 33(12), 2021.
- [12] Santiago Muñoz-Landin, Alexander Fischer, Viktor Holubec, and Frank Cichos. Reinforcement learning with artificial microswimmers. *Science Robotics*, 6(52):eabd9285, 2021.
- [13] Simona Colabrese, Kristian Gustavsson, Antonio Celani, and Luca Biferale. Flow navigation by smart microswimmers via reinforcement learning. *Physical review letters*, 118(15):158004, 2017.
- [14] Simona Colabrese, Kristian Gustavsson, Antonio Celani, and Luca Biferale. Smart inertial particles. *Physical Review Fluids*, 3(8):084301, 2018.
- [15] Luca Biferale, Fabio Bonaccorso, Michele Buzzicotti, Patricio Clark Di Leoni, and Kristian Gustavsson. Zermelo’s problem: optimal point-to-point navigation in 2D turbulent flows using reinforcement learning. *Chaos: An Interdisciplinary Journal of Nonlinear Science*, 29(10), 2019.
- [16] Jaya Kumar Alageshan, Akhilesh Kumar Verma, Jérémie Bec, and Rahul Pandit. Machine learning strategies for path-planning microswimmers in turbulent flows. *Physical Review E*, 101(4):043110, 2020.

- [17] Francesco Borra, Luca Biferale, Massimo Cencini, and Antonio Celani. Reinforcement learning for pursuit and evasion of microswimmers at low reynolds number. *Physical Review Fluids*, 7(2):023103, 2022.
- [18] Lucas Amoudruz and Petros Koumoutsakos. Independent control and path planning of microswimmers with a uniform magnetic field. *Advanced Intelligent Systems*, 4(3):2100183, 2022.
- [19] Yuguang Yang, Michael A Bevan, and Bo Li. Hierarchical planning with deep reinforcement learning for 3d navigation of microrobots in blood vessels. *Advanced Intelligent Systems*, 4(11):2200168, 2022.
- [20] Pejhman Ghassemi, Jianting Wang, Anthony J Melchiorri, Jessica C Ramella-Roman, Scott A Mathews, James C Coburn, Brian S Sorg, Yu Chen, and T Joshua Pfefer. Rapid prototyping of biomimetic vascular phantoms for hyperspectral reflectance imaging. *Journal of biomedical optics*, 20(12):121312–121312, 2015.
- [21] Lucas Amoudruz, Athena Economides, Georgios Arampatzis, and Petros Koumoutsakos. The stress-free state of human erythrocytes: Data-driven inference of a transferable RBC model. *Biophysical Journal*, mar 2023.
- [22] Robert D Groot and Patrick B Warren. Dissipative particle dynamics: Bridging the gap between atomistic and mesoscopic simulation. *The Journal of chemical physics*, 107(11):4423–4435, 1997.
- [23] Lucas Amoudruz. *Simulations and Control of Artificial Microswimmers in Blood*. PhD thesis, ETH Zurich, 2022.
- [24] Alireza Yazdani, Mingge Deng, Bruce Caswell, and George Em Karniadakis. Flow in complex domains simulated by dissipative particle dynamics driven by geometry-specific body-forces. *Journal of Computational Physics*, 305:906–920, 2016.
- [25] Petr Karnakov, Fabian Wermelinger, Sergey Litvinov, and Petros Koumoutsakos. Aphros: High performance software for multiphase flows with large scale bubble and drop clusters. In *Proceedings of the Platform for Advanced Scientific Computing Conference*, pages 1–10, 2020.
- [26] Dmitry Alexeev, Lucas Amoudruz, Sergey Litvinov, and Petros Koumoutsakos. Mirheo: High-performance mesoscale simulations for microfluidics. *Computer Physics Communications*, 254:107298, 2020.
- [27] Andrew Y Ng, Daishi Harada, and Stuart Russell. Policy invariance under reward transformations: Theory and application to reward shaping. In *ICML*, volume 99, pages 278–287. Citeseer, 1999.
- [28] Guido Novati and Petros Koumoutsakos. Remember and forget for experience replay. In *Proceedings of the 36th International Conference on Machine Learning*, 2019.
- [29] Guido Novati, Lakshminarayanan Mahadevan, and Petros Koumoutsakos. Controlled gliding and perching through deep-reinforcement-learning. *Physical Review Fluids*, 4(9):093902, 2019.
- [30] Siddhartha Verma, Guido Novati, and Petros Koumoutsakos. Efficient collective swimming by harnessing vortices through deep reinforcement learning. *P. Natl. Acad. Sci.*, page 201800923, may 2018.
- [31] Ioannis Mandralis, Pascal Weber, Guido Novati, and Petros Koumoutsakos. Learning swimming escape patterns for larval fish under energy constraints. *Physical Review Fluids*, 6(9):093101, 2021.
- [32] Sergio M Martin, Daniel Wälchli, Georgios Arampatzis, Athena E Economides, Petr Karnakov, and Petros Koumoutsakos. Korali: Efficient and scalable software framework for bayesian uncertainty quantification and stochastic optimization. *Computer Methods in Applied Mechanics and Engineering*, 389:114264, 2022.

Supplementary Material: Path planning of magnetic microswimmers in capillaries with deep reinforcement learning

Lucas Amoudruz¹, Sergey Litvinov¹, and Petros Koumoutsakos^{1,*}

¹School of Engineering and Applied Sciences, Harvard University, Cambridge, MA 02138, United States.

*corresponding author: petros@seas.harvard.edu

April 4, 2024

1 Generation of the geometry

The geometric representation of the capillaries is generated from an explicit representation (triangle mesh) obtained from ref. [1]. The triangle mesh was smoothed with a Laplacian filter and simplified to keep 10% of the faces in *Meshlab* [2]. A signed distance function (SDF) was then generated from the triangle mesh on a domain of size $576 \times 528 \times 24$ (simulation units). The SDF takes into account the periodic images of the geometry. Furthermore, the SDF was merged with that of two cylinders that form the inlet and outlet of the geometry and are periodically connected (fig. 1). This periodic connection makes the domain fully periodic and simplifies particle simulations as no mechanism of inserting and deleting particles is needed.

The SDF geometric representation is usable by both *Aphros* [3] and *Mirheo* [4] to perform the Stokes and the detailed blood simulations, respectively. Furthermore it simplifies the implementation of the bounce-back of the swimmer in the simplified model, as a evaluating the SDF at the swimmer's position indicates if it is inside or outside of the capillaries. In the latter case, the swimmer is simply put to its previous position.

Figure 2 shows a two-dimensional slice of the velocity field obtained from *Aphros*. This field corresponds to an inlet of unit velocity and no-slip along the walls of the capillaries, and we assumed an incompressible, Newtonian fluid. This velocity field is used by the simplified model described in the main text.

2 Calibration of the simplified model

We consider an artificial bacterial flagellum (ABF) of radius $r = 2 \mu\text{m}$ and length $l = 18.37 \mu\text{m}$ in a magnetic field that rotates with a frequency $f = 1 \text{ kHz}$. We define the angular frequency $\omega = 2\pi f$. The swimming speed of the ABF in blood is measured from 15 simulations with different initial cells configurations. The simulations consist of a single ABF swimming in a periodic tube of radius $R = 10 \mu\text{m}$ (fig. 3). The tube is filled with a suspension of blood cells at $\text{Ht} = 25\%$ and the ABF is initially placed at the center of the tube. We find a swimming speed of $U = 8.40 \times 10^{-3} l \omega \approx 1 \text{ mm s}^{-1}$ and a diffusion coefficient (due to collisions with the surrounding cells) of $D = 2.56 \times 10^{-4} l^2 \omega \approx 542 \mu\text{m}^2/\text{s}$.

In the reduced order model, this corresponds to $U \approx U_{in} = 1$, where U_{in} is the average velocity at the inlet and $D_{\text{sim}} \approx 0.0123$ in simulation units. The noise is anisotropic and to account for the differences we use a larger value during training $D = 0.1 \approx 8.14 D_{\text{sim}}$. Furthermore, we set $U = 0.4 U_{in}$ in the simplified model, making the task more difficult but potentially more robust to the ABF being stuck by the surrounding cells.

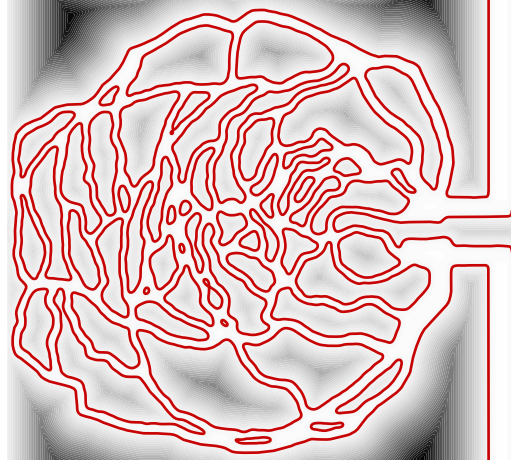


Figure 1: Slice of the SDF of the capillaries (grey scale) and corresponding zero-isoline (solid line).

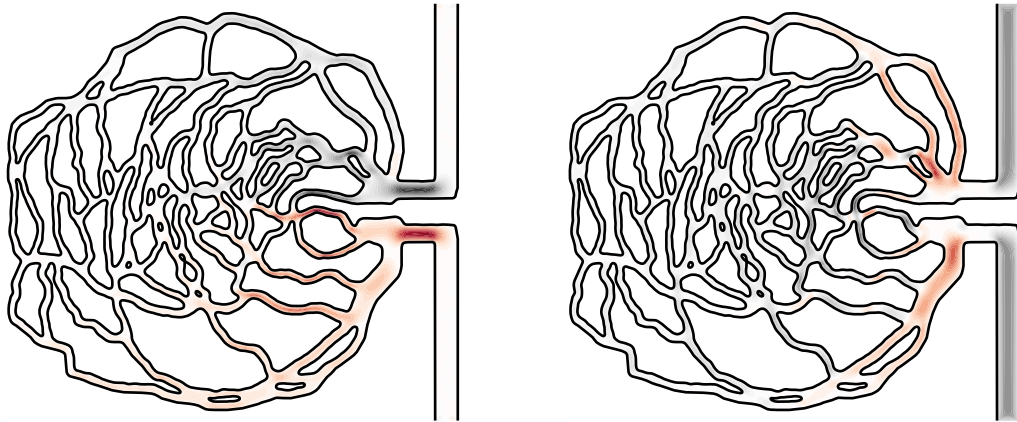


Figure 2: Slice of the velocity inside the capillaries obtained from the Stokes solver *Aphros*. The left and right plots correspond to the x and y components, respectively, and the solid line denotes the boundaries of the walls.

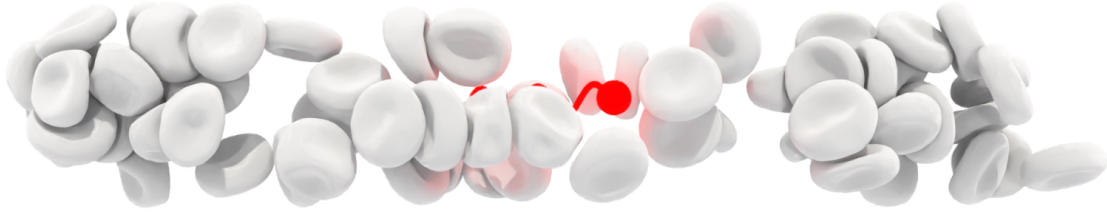


Figure 3: Simulation snapshot of an ABF inside a periodic tube (tube boundaries not shown).

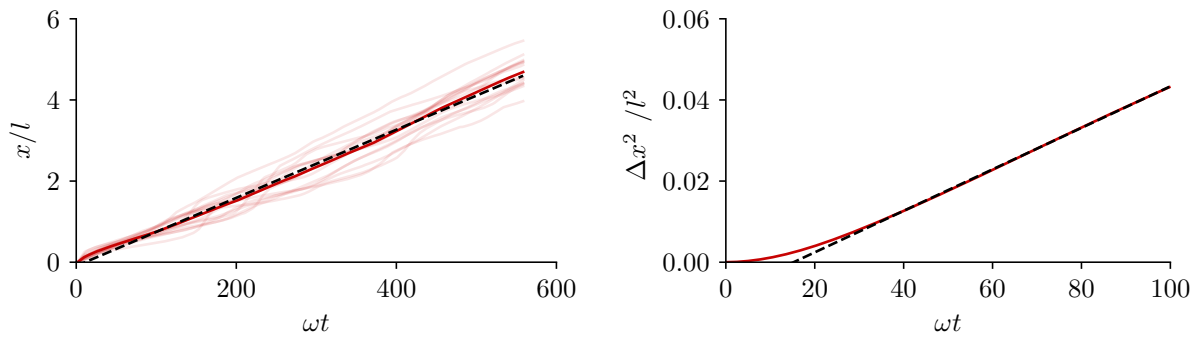


Figure 4: Left: Displacement of the ABFs for 15 simulations (shaded lines) against time. The solid line corresponds to the average displacement and the dashed line is a linear fit to this line. Right: Mean squared displacement of the 15 ABFs along the x axis against time (solid line) and linear fit of the non ballistic part (dashed line).

3 Hyper-parameters in the reinforcement learning setup

Each episode is ended when either the ABF reaches the target within a distance $\delta = 5$ or the simulation time is larger than $T_{\max} = 500$. Actions are computed from the state every $\Delta t = 0.1$. The agent was trained with a self propelling speed of $U = 0.2$ and a noise level of $D = 0.1$, and the maximal velocity at the inlet was set to 1. The discount factor was set to $\gamma = 1$ and we used $C = 1$ in the reward equation.

We used the default settings in *Korali* [5]. The initial exploratory noise level was set to 0.1 along each action direction. We used the Adam optimizer with a learning rate of 1×10^{-4} and a mini-batch size of 128. The parameters of the policy were updated after every experience. The replay memory has a size of 131072. The REFER parameters [6] were set to $\beta = 0.3$, $C_{\max} = 4$, $D = 0.1$, $A = 0$. The policy is represented by a neural network with 2 hidden layers of 64 units each, separated by a tanh activation function.

References

- [1] Pejman Ghassemi, Jianting Wang, Anthony J Melchiorri, Jessica C Ramella-Roman, Scott A Mathews, James C Coburn, Brian S Sorg, Yu Chen, and T Joshua Pfefer. Rapid prototyping of biomimetic vascular phantoms for hyperspectral reflectance imaging. *Journal of biomedical optics*, 20(12):121312–121312, 2015.
- [2] Paolo Cignoni, Marco Callieri, Massimiliano Corsini, Matteo Dellepiane, Fabio Ganovelli, Guido Ranzuglia, et al. Meshlab: an open-source mesh processing tool. In *Eurographics Italian chapter conference*, volume 2008, pages 129–136. Salerno, Italy, 2008.
- [3] Petr Karnakov, Fabian Wermelinger, Sergey Litvinov, and Petros Koumoutsakos. Aphros: High performance software for multiphase flows with large scale bubble and drop clusters. In *Proceedings of the Platform for Advanced Scientific Computing Conference*, pages 1–10, 2020.
- [4] Dmitry Alexeev, Lucas Amoudruz, Sergey Litvinov, and Petros Koumoutsakos. Mirheo: High-performance mesoscale simulations for microfluidics. *Computer Physics Communications*, 254:107298, 2020.
- [5] Sergio M Martin, Daniel Wälchli, Georgios Arampatzis, Athena E Economides, Petr Karnakov, and Petros Koumoutsakos. Korali: Efficient and scalable software framework for bayesian uncertainty quantification and stochastic optimization. *Computer Methods in Applied Mechanics and Engineering*, 389:114264, 2022.
- [6] Guido Novati and Petros Koumoutsakos. Remember and forget for experience replay. In *Proceedings of the 36th International Conference on Machine Learning*, 2019.